THE JOURNAL OF PHYSICAL CHEMISTRY C LETTERS

2007, *111,* 1874−1877
Published on Web 01/18/2007

Atomic-Scale View of Redox-Induced Reversible Changes to a Metal-Oxide Catalytic Surface: VO_x/α-$Fe_2O_3(0001)$

Chang-Yong Kim,[†,§] Anthony A. Escuadro,[†] Peter C. Stair,[‡] and Michael J. Bedzyk*[,†]

Department of Materials Science and Engineering, and Department of Chemistry, Northwestern University, Evanston, Illinois 60208

Received: November 27, 2006; In Final Form: December 31, 2006

X-ray standing wave (XSW) analysis and X-ray photoelectron spectroscopy are used to trace the electronic and atomic-scale structural changes of a supported vanadium oxide system at different stages of its oxidation−reduction cycle. Both the oxidation state and adsorption geometry of the vanadium oxide and its α-Fe_2O_3-(0001) single crystal support show reversible changes through the oxidation−reduction cycle characteristic of catalytic behavior. The 3D V atomic distribution maps, derived from the summation of the XSW measured Fourier components, reveal that the V undergoes adsorption site exchange during the oxidation and reduction cycle.

Introduction

Metal oxide monolayers or clusters anchored to an oxide support are important catalysts for hydrocarbon transformations, and among these materials supported vanadium oxide has received the most attention in the scientific literature because of its significance for industrial catalytic processes.[1] In spite of extensive efforts to define the molecular structure of supported metal oxides (such as vanadium oxide), there has yet to be any direct, experimental information on the atomic positions of the metal cations on the support. Moreover, recent experiments clearly indicate that oxidation-state changes in a supported oxide catalyst during reduction−oxidation (redox) reactions accompany atomic-scale structure changes.[2−6]

Herein, we present detailed measurements of the V atomic positions for supported vanadium oxide as a function of the vanadium oxidation state. A general consensus for the atomic-scale structure of supported vanadium oxide, formed by numerous experiments, is that it exists as an isolated or polymerized VO_4 unit.[7] However, studies for the positions of vanadium cations with respect to the support and its sensitivity to the oxidation−reduction cycle, at the atomic scale, are rare. For vanadium oxides supported on γ-Al_2O_3, Ruitenbeek et al. reported substantial changes in V K-edge absorption spectra after reduction by CO and proposed migration of V^{3+} into γ-Al_2O_3 lattice.[5] Change of a dehydrated, isolated VO_4 monomer to a polymeric gel after room-temperature hydration and partial restoration to a monomer by dehydration has been observed with Raman spectroscopy for vanadium oxides supported on silica.[6] Recently, local structures of V coexisting in different oxidation states on TiO_2(110) have been studied with X-ray standing wave (XSW) analysis.[8]

In the present study, we obtained the oxidation-state-dependent atomic positions by using a combined XSW and X-ray photoelectron spectroscopy (XPS) approach applied in situ to an ultrahigh vacuum prepared vanadium oxide supported on an α-Fe_2O_3 (hematite) (0001) single-crystal surface.

Experimental Methods

The $10 \times 10 \times 1$ mm^3 α-Fe_2O_3(0001) single-crystal surfaces were cleaned in ultrahigh vacuum (UHV) by annealing at 450 °C in an atomic oxygen beam. The atomic oxygen and atomic hydrogen were produced by passing the molecular species through a hot refractory metal tube. Vanadium was deposited onto a clean α-Fe_2O_3(0001) surface from a high-temperature K-cell evaporation source of vanadium metal with sample at room temperature. During vanadium deposition, the pressure was typically 2×10^{-9} Torr. The oxidation and subsequent reduction of the V/α-Fe_2O_3(0001) was achieved by exposure to atomic oxygen and atomic hydrogen, respectively, while the sample was kept at room temperature. Because the deposition, oxidation, and reduction of vanadium occurred at room temperature, thermal diffusion of adsorbed vanadium was minimized.

X-ray photoelectron spectroscopy (XPS) and X-ray standing wave (XSW) measurements were conducted in two separate UHV chambers with base pressures of 5×10^{-11} and 2×10^{-10} Torr, respectively. The XPS measurements used Al Kα radiation (without a monochromator) and a hemispherical analyzer for photoelectron energy analysis. The XSW measurements were conducted at the Advanced Photon Source (APS) 5ID-C beamline[9] and used an X-ray fluorescence (XRF) solid-state detector to monitor the V Kα XRF yield. The vanadium surface coverage, determined by ex situ Rutherford backscattering spectroscopy (RBS) measurements, was 0.5 monolayer (ML). The coverage of 1 ML is defined as the area density of Fe ions in the (0001) surface, 9.1 atoms/nm^2. An XSW measurement monitors the XRF yield of a selected atomic species while

* Corresponding author. E-mail: bedzyk@northwestern.edu.
† Department of Materials Science and Engineering.
‡ Department of Chemistry.
§ Current address: Canadian Light Sources Inc. E-mail: Chang-Yong.Kim@lightsource.ca.

10.1021/jp067862s CCC: $37.00

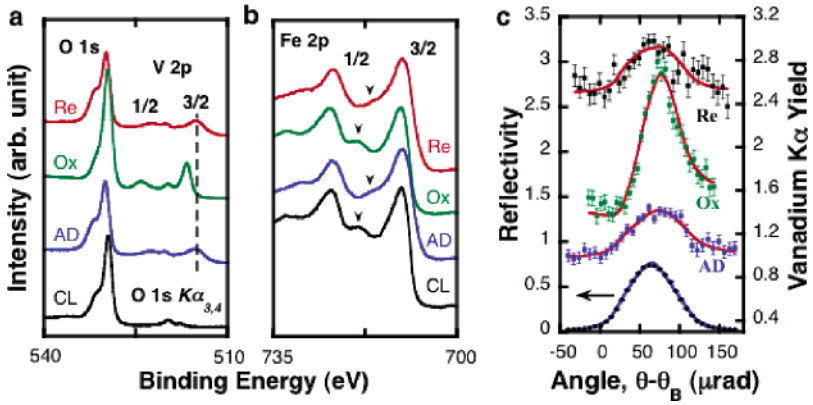

Figure 1. X-ray photoelectron spectra of (a) O 1s, V 2p and (b) Fe 2p taken with an electron takeoff angle of 20° from the sample surface. (a and b) The XPS spectra are displaced vertically in the order of processing; starting with the clean substrate spectra (CL), followed by the vanadium film as-deposited (AD), oxidized by atomic oxygen (Ox), and reduced by atomic hydrogen (Re). (a) Dashed line is drawn to aid peak position comparison. (b) Arrows between the $2p_{1/2}$ and $2p_{3/2}$ peaks mark satellite peaks originating from Fe^{2+} (AD and Re) or Fe^{3+} (CL and Ox). (c) X-ray standing wave data and analysis for the (10$\bar{1}$4) Bragg reflection showing the angle θ dependence of the reflectivity (bottom) and vanadium Kα fluorescence yields for the AD, Ox, and Re processing steps. The Ox and Re curves are vertically offset for clarity.

scanning in angle through an *hkl* substrate Bragg reflection.[10−13] The modulation of the XRF yield directly measures the amplitude (f_H) and phase (P_H) of the $H = hkl$ Fourier component of the atom density distribution. As demonstrated recently, a summation of these XSW measured Fourier components generates an element-specific real-space 3D atomic map.[12,14−18]

Results and Discussion

From our "in-house" XPS data in Figure 1a, the as-deposited vanadium has its $2p_{3/2}$ photoelectron binding energy (BE) at 515.3 eV corresponding to a 3+ oxidation state. Reported values for various vanadium oxides are V^{3+} at 515.85 eV and V^{5+} at 517.2 eV.[19] The as-deposited surface was exposed to atomic oxygen to produce a vanadium oxidation state of +5 (BE 516.9 eV). Exposure to atomic hydrogen reduced the vanadium cations back to 3+ (BE 515.3 eV). The oxygen 1s photoelectron intensity is attenuated slightly after V deposition and then substantially increased after atomic oxygen exposure. These intensity variations can be explained by the covering of surface oxygen with V and then the addition of oxygen at the topmost surface, respectively. The oxidation state changes involve the transfer of electrons between adsorbed vanadium and substrate Fe, which can be seen in the Fe 2p XPS from the interface Fe ions in Figure 1b, where the 3+ main peaks (1/2 and 3/2) are at a 1 eV lower BE relative to the 2+, and the satellite peak (between the main peaks) shifts in the same direction by 2 eV. A fraction of the Fe ions in the 3+ oxidation state[20] was reduced to the 2+ oxidation state by accepting electrons donated by adsorbed vanadium. The reduced Fe ions were reoxidized to 3+ concurrently with oxidation of the deposited vanadium to 5+. The atomic hydrogen exposure caused a reduction of the α-Fe_2O_3(0001) substrate just as in the as-deposited case. These electronic structure data therefore establish a key aspect of catalytic behavior: coupled cyclic behavior of both vanadium and iron during oxidation and reduction of supported vanadium.

The V adsorption geometry also shows a clear reversible cycle as seen in the (10$\bar{1}$4) XSW measurements (Figure 1c) from the different oxidation states synchronous with these electronic structure changes. Table 1 summarizes the XSW analysis results from the as-deposited, oxidized, and reduced V/α-Fe_2O_3(0001) surfaces. Note that our XSW and XPS results for the as-deposited and reduced surfaces are equivalent, indicating that these two surfaces are essentially identical. Aggregation of vanadium oxide has been reported for the case of reduction at a high temperature.[21] However, in the present study the entire process occurred at room temperature and therefore it should be safe to assume that the as-deposited and reduced surfaces are identical.

TABLE 1: Summary of the XSW Experimental (exptl) Results from the As-Deposited (AD), Oxidized (Ox), and Reduced (Re) Surface Treatments of the 0.5 ML V/ α-Fe_2O_3(0001) Surface[a]

	(0006)		(10$\bar{1}$4)		(01$\bar{1}$2)	
(*hkil*)	f_H	P_H	f_H	P_H	f_H	P_H
exptl AD	0.19(5)	1.04(3)	0.31(2)	0.30(2)	0.39(2)	0.22(2)
model Re	0.14	1.06	0.20	0.29	0.45	0.16
exptl Ox	0.22(5)	0.91(3)	0.41(2)	0.53(1)	0.27(4)	0.32(2)
model Ox	0.26	0.88	0.39	0.53	0.22	0.30
exptl Re	0.22(5)	1.02(5)	0.30(3)	0.28(1)		

[a] The measured f_H and P_H values for V from three different $H = (hkil)$ Bragg reflections are compared to those calculated from the two best-fit models described in Figure 3.

The Fourier inversion using the XSW measured f_H and P_H values generates the XRF-selected 3D atomic density map with a periodicity imposed by the primitive unit cell of the substrate. Figure 2 shows the 2D cuts through the reduced and oxidized 3D V atomic density maps, which makes it possible to identify the adsorption sites and their relative occupancies in a model-independent way. The high-symmetry V adsorption sites, which are compatible with the images, are labeled as A, B, and C in Figure 2. Note that the "effective" primitive unit cell causes the C site to be folded into a position directly below the A site (see the Supporting Information); these two sites are not fully resolved, but simultaneous occupation of the two results in a distinct vertical broadening of the V density distribution. The maps clearly show a build-up of V density at the A and C sites for the reduced surface and at the A and B sites for the oxidized surface.

For the α-Fe_2O_3(0001) surface, there are two high-symmetry Fe sites (A and B) above the topmost oxygen layer that are symmetrically equivalent to the Fe occupied octahedral sites in the bulk. The A site is located closer to the underlying oxygen layer than the B site. The C site, another high-symmetry surface site, is also a bulk octahedral site but is not occupied in the bulk by Fe due to stoichiometry.

To quantify the occupation fractions and exact heights for sites A, B, and C, we performed a least-squares fit of a model to the measured f_H and P_H sets for each surface. The model has

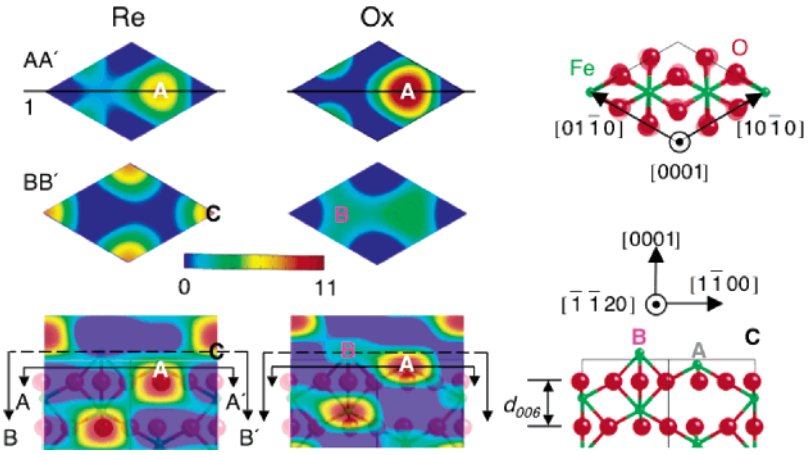

Figure 2. The (0001) (top) and ($\bar{1}\bar{1}$20) (bottom) 2D cuts through the XSW measured 3D vanadium atomic density maps for the reduced (Re) and oxidized (Ox) V/α-Fe_2O_3(0001) surface and projections of the α-Fe_2O_3 ball and stick model on the right. The map for the as-deposited surface is equivalent to Re. The solid line labeled 1 indicates the position of the ($\bar{1}\bar{1}$20) cut-plane shown in the side view, lines AA′ and BB′ indicate the positions of the (0001) cut-planes shown in the top views. As a reference, the ($\bar{1}\bar{1}$20) projection of the α-Fe_2O_3 structure is overlapped with the 2D cuts in the bottom. The high-symmetry sites A, B, and C are indicated.

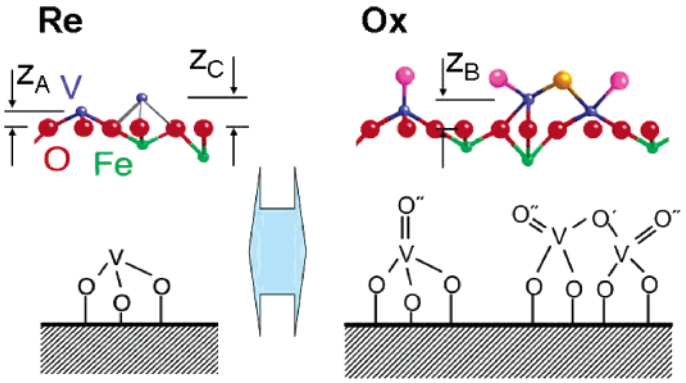

Model	c_A	c_B	c_C	z_A(Å)	z_B(Å)	z_C(Å)
Re	0.33(2)	0	0.27(2)	0.6(3)	-	1.6(3)
Ox	0.33(1)	0.08(1)	0	0.7(1)	1.6(4)	-

Figure 3. Top: Model proposed for the (Re) reduced vanadium oxide, (Ox) fully oxidized vanadium oxide in polymeric and isolated VO_4 form, and schematic diagram of each oxide form (reduced, polymerized, and isolated vanadium oxide). Oxygen atoms in double bond to V, V−O−V, and V−O−support are denoted by O″, O′, and O, respectively. Bottom: Best-fit parameters for V adsorption geometry models; c_j is the fraction of V atoms occupying the j = A, B, or C site, and z_j is the corresponding height.

six parameters: c_A, c_B, and c_C represent the fractions of V atoms occupying site A, B, and C, and z_A, z_B, and z_C are the respective adsorption heights of V atoms above the unrelaxed oxygen plane. On the basis of this model, the Hth Fourier component for the V atomic distribution is

$$F_H = f_H \exp(2\pi\, iP_H) = \sum_j c_j \exp(2\pi\, i\mathbf{H}\cdot\mathbf{r}_j) \qquad (1)$$

where index j is summed over the three sites (A, B, and C) and vector $\boldsymbol{r}_j$ locates the V atom at the jth site. By inspection of the V atomic density maps (Figure 2), it was possible to set c_B = 0 for the reduced surface and c_C = 0 for the oxidized surface. The parameters from the best-fits, which are listed at the bottom of Figure 3, quantitatively demonstrate that oxidation of the vanadium causes no change to the V atoms in the A sites but does cause V atoms in C sites to vacate C sites and partially redistribute to B sites. The concurrent oxidation to V^{5+} and Fe^{3+} caused V atoms in C sites to move to B sites with a XSW measured adsorption height coincidentally equivalent to that of the C site. (Note that the B and C sites have distinct lateral positions that are sensed by the XSW 3D image.) The XSW analysis determines the fraction of V atoms, $C = (c_A + c_B + c_C)$, that are incorporated in 2D surface sites A, B, and C (60% for the reduced surface and 41% for the oxidized surface). The remaining V atoms are measured by XSW to be in a "random" distribution relative to the substrate lattice. This random fraction (1-C), which could include VO_x nanoparticles and V in defect sites, does not influence the structural determination of the nonrandom vanadium.

The reducibility of the substrate has significant effects in heterogeneous catalysis.[22] Yet the reducible substrate is typically considered as an electron reservoir from which the catalysts can easily remove or acquire electrons. This present study shows that the electronic and atomic structures of the catalyst and the support are entangled such that their mutual influences are inseparable.

Previous spectroscopy studies of supported vanadium oxide, with vanadium in the 5+ oxidation state, have proposed that

an isolated VO_4 unit exists at lower coverages and a polymerized form exists at higher coverages.[1,7,23]

Fully dispersed vanadium oxide on various oxide-supports has been reported to have a maximum vanadium coverage of 5−7 atoms/nm^2 beyond which a crystalline V_2O_5 formation is initiated.[24,25] SiO_2 has been known to accommodate only isolated vanadyl units with a maximum achievable coverage reported to be 2−3 V atoms/nm^2.[26] The vanadium coverage in our present study is 4.1/nm^2 (one vanadium atom within a 1×1 α-Fe_2O_3-(0001) surface unit cell) where one can expect polymerized dispersed vanadium oxides.[24,25]

In Figure 3, atomic-scale structures of surface vanadium oxide in reduced and oxidized form are proposed based on the XSW and XPS results. Vanadium in the 3+ oxidation state (reduced form) occupies A and C sites, which correspond to surface hollow sites. Oxidized vanadium ions (V^{5+}) either make a double bond with oxygen (A site) or form a polymeric surface vanadium oxide by mimicking an unrelaxed bulk α-Fe_2O_3 structure (A and B sites). Because at this stage our direct structural information is only for the V ions, the bonding geometry of oxygen in this model is based on chemical intuition, and further experimental and/or theoretical studies are required to locate oxygen atoms especially in the polymerized form.

The present results demonstrate a new in situ approach for directly observing the coupled changes in electronic and atomic-scale geometrical structure at various stages of surface catalytic reactions. In the future, this new approach can be extended to reactions under atmospheric gas environments and can be compared to other in situ techniques. The method can be applied to various surface chemical reaction studies, for example, identification of active site(s) in heterogeneous catalysis and atomic-scale investigations of the nucleation and growth of nanostructured films, such as metal nanoparticles on oxide surfaces.

Acknowledgment. We thank the DND-CAT staff and Zhan Zhang for technical assistance, and Paul Fenter for helpful scientific discussions. This work was supported by the DOE under contract No. DE-FG02-03ER15457 to the Institute for Catalysis in Energy Processes (ICEP) at Northwestern University (NU). Use of the APS at Argonne National Laboratory was supported by the DOE-BES under Contract No. W-31-109-ENG-38. DND-CAT is supported in part by the State of Illinois. This work made use of NU Central Facilities supported by the MRSEC through NSF Contract No. DMR-0520513.

Supporting Information Available: Construction of three-dimensional atomic density map. This material is available free of charge via the Internet at http://pubs.acs.org.

References and Notes

(1) Weckhuysen, B. M.; Keller, D. E. *Catal. Today* **2003**, *78*, 25.

(2) Ackermann, M. D.; Pedersen, T. M.; Hendriksen, B. L. M.; Robach, O.; Bobaru, S. C.; Popa, I.; Quiros, C.; Kim, H.; Hammer, B.; Ferrer, S.; Frenken, J. W. M. *Phys. Rev. Lett.* **2005**, *95*, 255505.

(3) Giorgio, S.; Sao Joao, S.; Nitsche, S.; Chaudanson, D.; Sitja, G.; Henry, C. R. *Ultramicroscopy* **2006**, *106*, 503.

(4) Ketteler, G.; Ogletree, D. F.; Bluhm, H.; Liu, H.; Hebenstreit, E. L. D.; Salmeron, M. *J. Am. Chem. Soc.* **2005**, *127*, 18269.

(5) Ruitenbeek, M.; Dillen, A. J. v.; Groot, F. M. F. d.; Wachs, I. E.; Geus, J. W.; Koningsberger, D. C. *Top. Catal.* **2000**, *10*, 241.

(6) Xie, S.; Iglesia, E.; Bell, A. T. *Langmuir* **2000**, *16*, 7162.

(7) Wachs, I. E. *Catal. Today* **2005**, *100*, 79.

(8) Kroger, E. A.; Allegretti, F.; Knight, M. J.; Polcik, M.; Sayago, D. I.; Woodruff, D. P.; Dhanak, V. R. *Surf. Sci.* **2006**, *600*, 4813.

(9) Walko, D. A.; Sakata, O.; Lyman, P. F.; Lee, T.-L.; Tinkham, B. P.; Okasinski, J. S.; Zhang, Z.; Bedzyk, M. J. *AIP Conf. Proc.* **2004**, *705*, 1166.

(10) Golovchenko, J. A.; Patel, J. R.; Kaplan, D. R.; Cowan, P. L.; Bedzyk, M. J. *Phys. Rev. Lett.* **1982**, *49*, 560.

(11) Zegenhagen, J. *Surf. Sci. Rep.* **1993**, *18*, 199.

(12) Bedzyk, M. J.; Cheng, L. W. *Rev. Mineral. Geochem.* **2002**, *49*, 221.

(13) Woodruff, D. P. *Rep. Prog. Phys.* **2005**, *68*, 743.

(14) Cheng, L.; Fenter, P.; Bedzyk, M. J.; Sturchio, N. C. *Phys. Rev. Lett.* **2003**, *90*, 255503.

(15) Escuadro, A. A.; Goodner, D. M.; Okasinski, J. S.; Bedzyk, M. J. *Phys. Rev. B* **2004**, *70*, 235416.

(16) Okasinski, J. S.; Kim, C.-Y.; Walko, D. A.; Bedzyk, M. *J. Phys. Rev. B* **2004**, *69*, 041401.

(17) Zhang, Z.; Fenter, P.; Cheng, L.; Sturchio, N. C.; Bedzyk, M. J.; Machesky, M. L.; Wesolowski, D. J. *Surf. Sci.* **2004**, *554*, L95.

(18) Kim, C.-Y.; Elam, J. W.; Pellin, M. J.; Goswami, D. K.; Christensen, S. T.; Hersam, M. C.; Stair, P. C.; Bedzyk, M. J. *J. Phys. Chem. B* **2006**, *110*, 12616.

(19) Demeter, M.; Neumann, M.; Reichelt, W. *Surf. Sci.* **2000**, *454*, 41.

(20) Rao, C. N. R.; Raveau, B. *Transition Metal Oxides: Structure, Properties, and Synthesis of Ceramic Oxides*; Wiley-VCH: New York, 1998.

(21) Baares, M. A.; Cardoso, J. H.; Agulló-Rueda, F.; Correa-Bueno, J. M.; Fierro, J. L. G. *Catal. Lett.* **2000**, *64*, 191.

(22) Magg, N.; Giorgi, J. B.; Schroeder, T.; Baumer, M.; Freund, H. J. *J. Phys. Chem. B* **2002**, *106*, 8756.

(23) Wachs, I. E.; Weckhuysen, B. M. *Appl. Catal., A* **1997**, *157*, 67.

(24) Deo, G.; Wachs, I. E. *J. Catal.* **1994**, *146*, 323.

(25) Wachs, I. E. *Catal. Today* **1996**, *27*, 437.

(26) Das, N.; Eckert, H.; Hu, H. C.; Wachs, I. E.; Walzer, J. F.; Feher, F. J. *J. Phys. Chem.* **1993**, *97*, 8240.